ADVANCED FUNCTIONAL MATERIALS
www.afm-journal.de

Polyol Synthesis of Ultrathin Pd Nanowires via Attachment-Based Growth and Their Enhanced Activity towards Formic Acid Oxidation

*Yi Wang, Sang-Il Choi, Xin Zhao, Shuifen Xie, Hsin-Chieh Peng, Miaofang Chi, Cheng Zhi Huang, and Younan Xia**

Palladium wavy nanowires with an ultrathin diameter of 2 nm are synthesized using the polyol method without the involvement of any template. The success of this synthesis relies on the use of a suitable precursor that could be reduced instantaneously to generate a large number of small Pd nanoparticles. Due to a quick depletion of precursor, the small nanoparticles were unable to grow in size through atomic addition. In the case of low surface charges and high surface energies, these small nanoparticles were forced to coalesce into ultrathin nanowires with a wavy morphology via an attachment mechanism. Thanks to the unique structure and involvement of twin defects, the as-obtained Pd ultrathin nanowires show a catalytic current density of 2.5 times higher than the conventional Pd/C catalyst towards formic acid oxidation. This work not only offers a powerful route to the synthesis of nanowires through attachment-based growth but also opens the door to the rational design and fabrication of novel metal nanostructures with enhanced properties.

1. Introduction

Controlling the shape and size of metal nanocrystals has received extensive attention in recent years since these two parameters allow people to tailor the properties of nanocrystals and thus enhance their performances in a variety of applications.[1] Among various methods for metal nanocrystals, solution-phase synthesis is considered to be the most promising route because of its capability to precisely control both the shape and size of nanocrystals. It has been demonstrated that the formation of metal nanocrystals in a solution phase involves both nucleation and growth steps.[2] Specifically, zero-valent metal atoms can be generated via either the decomposition or reduction of a precursor compound, which then aggregate into small clusters (or nuclei) once their concentration has reached supersaturation. When the concentration of atoms quickly drops below the level of supersaturation, nucleation can no longer occur and the newly formed atoms will be added onto the nuclei. As a result, the nuclei will grow into larger nanocrystals with various shapes or morphologies as controlled by thermodynamics or kinetics. At the same time, Ostwald ripening, dissolution of small nanoparticles and re-deposition of the dissolved species onto the surfaces of larger ones, can also occur in a solution-phase synthesis in an effort to minimize the total interfacial free energy of the system.[3] Thanks to the efforts from many research groups, metal nanocrystals with a myriad of different shapes or morphologies have been successfully designed and synthesized.

In addition to the traditional mechanism involving various atomic species, a new growth pathway was proposed by Penn and Banfield in 1998, which is known as "oriented attachment".[4] In this new pathway, small nanoparticles are formed and then forced to coalesced into larger structures by sharing planes with a common crystallographic orientation. In this case, the fusion of two particles will eliminate the high energy facets and thus reduce the total interfacial free energy of the system. To date, there have been many successful demonstrations of oriented attachment for the facile synthesis of anisotropic semiconducting quantum dots and oxides,[5] in which attachment is mainly driven by the permanent or temporary electric or magnetic dipoles. In comparison, utilization of the attachment mechanism for noble-metal nanostructures is more challenging because metal nanoparticles do not have permanent dipoles. Nevertheless, a number of studies have

Y. Wang, Dr. S.-I. Choi, X. Zhao, S. Xie, Prof. Y. Xia
The Wallace H. Coulter
Department of Biomedical Engineering
Georgia Institute of Technology and Emory University
Atlanta, Georgia 30332, USA
E-mail: younan.xia@bme.gatech.edu
Y. Wang, Prof. C. Z. Huang
Education Ministry Key Laboratory on Luminescence and Real-Time Analysis
School of Chemistry and Chemical Engineering
Southwest University
Chongqing, 400715, PR China
H.-C. Peng, Prof. Y. Xia
School of Chemistry and Biochemistry
Georgia Institute of Technology
Atlanta, Georgia 30332, USA
Dr. M. Chi
Materials Science and Technology Division
Oak Ridge National Laboratory
Oak Ridge, Tennessee 37830, USA

DOI: 10.1002/adfm.201302339

demonstrated the ability to generate metal nanostructures through the attachment mechanism. For example, Ozaki, Yang, and their co-workers observed the attachment-based assembly of Ag nanocrystals into dendritic Ag nanostructures.[6] Ma and co-workers prepared Ag nanorices through attachment-dominated anisotropic growth along the <111> direction.[7] Halder and Ravishankar synthesized ultrafine single-crystalline Au nanowires via attachment,[8] and our group recently also obtained Au wavy nanowires at the air/water interface through attachment and cold welding.[9] Yang and co-workers obtained Pt-Ag alloy nanowires in the presence of oleylamine and oleic acid through oriented attachment, and found that the formation of such nanowires was greatly dependent on the composition of Pt and Ag.[10] Li and co-workers prepared worm-like nanowires of Pt-M (M = Cu, Co, Ni, Fe) alloys through the attachment of small nanoparticles.[11] Most recently, Lou, Wang, and their co-workers reported the fabrication of ultrathin and very long single-crystal Pt, Pt-Au, and Pt-Pd nanowires via attachment using a solvothermal method.[12] Of particular interest, Zheng and co-workers reported the first direct observation of the metal nanoparticles undergoing oriented attachment and thus the formation of Pt_3Fe nanorods, achieved by using a real-time transmission electron microscopy (TEM) imaging technique.[13] This work not only directly confirmed the attachment mechanism involved in the formation of one-dimensional metal nanostructures but also paved the way for the rational design of other types of anisotropic nanomaterials with controlled properties. In spite of these reports on the growth of anisotropic metal nanostructures via particle attachment, a complete understanding of the details is still lacking, including the driving force, the influencing factors, and the relationship between the reaction kinetics and particle attachment.

In the present work, we studied the relationship between the reaction kinetics and the tendency of attachment by using Pd as a model system. We demonstrated that a fast reduction has to be used in order to generate a large number of small nanoparticles and, at the same time, complete depletion of the precursor helps terminate the growth pathway via atomic addition. When $(CF_3COO)_2Pd$ was employed as a precursor, we successfully achieved the synthesis of ultrathin Pd wavy nanowires in high purity in a number of different polyols. Owing to the fast reaction associated with $(CF_3COO)_2Pd$, nucleation burst occurred within a very short period of time after the precursor had been introduced into the polyol. As a result, a large number of small and uniform Pd nanoparticles with a diameter of 2–3 nm were generated in the early stage of the synthesis. These small Pd nanoparticles were unstable at relatively high temperatures due to their high surface free energies and low surface charges, and thus had a strong tendency to coalesce into wavy nanowires through an attachment pathway. Our mechanistic studies indicated that both the fast reaction kinetics during nucleation and the low surface charge played important roles in the attachment process and thus the formation of anisotropic Pd nanowires in high yield. In addition, our electrochemical measurements indicated that the as-obtained Pd wavy nanowires showed a catalytic current density 2.5 times higher than the conventional Pd/C catalyst towards formic acid oxidation (FOR) reaction.

2. Results and Discussion

2.1. Synthesis of Pd Ultrathin Nanowires

In a typical synthesis, poly(vinyl pyrrolidone) (PVP) (colloidal stabilizer) and $(CF_3COO)_2Pd$ (precursor) were dissolved separately in diethylene glycol (DEG) (solvent and reductant). The solution containing $(CF_3COO)_2Pd$ was quickly injected into the PVP solution at 140 °C under magnetic stirring. The solution turned into black immediately after the introduction of precursor, implying the formation of Pd nanoparticles due to the reduction of $(CF_3COO)_2Pd$ by DEG. The reaction was terminated after 3 h, and Pd nanowires with a wavy morphology were obtained. **Figure 1**a and b shows TEM images of a typical sample of the Pd nanowires under low- and high-magnifications, respectively. The TEM images indicated that the Pd wavy nanowires were obtained with a high purity approaching 100%. The nanowires were 2.0 ± 0.6 nm in width and several tens to hundreds of nanometers in length. Figure 1c shows high-resolution bright-field scanning transmission electron microscopy (BF-STEM) image of the Pd nanowires, where the lattice fringes could be clearly resolved. The lattice spacing of each group of parallel fringes was 0.23 nm, corresponding to the (111) planes of face-centered cubic (*fcc*) Pd. It should be noted that each nanowire was composed of a number of interconnected, single-crystal building blocks, which merged together from different angles. As a result, twin defects could be readily observed along each nanowire where coalescence took place. The high-resolution high-angle annular dark-field STEM (HAADF-STEM) images recorded from two individual Pd nanowires are shown in Figure 1d and e, respectively, further revealing that the coalescence between two building blocks could involve single-crystal structure with the same lattice plane or twin boundaries (TB). X-ray diffraction (XRD) pattern shown in Figure S1 of the Supporting Information indicated that the as-obtained nanowires were composed of the element Pd only, because all the diffraction peaks could be indexed to the *fcc* Pd (JCPDS No. 05–0681). The broadening of the peaks can be attributed to the relatively small cross sections of the nanowires.[14]

Except for DEG, other polyols with different lengths of hydrocarbon chains could also be used as both the reductant and solvent for the synthesis of Pd nanowires using the same protocol. As shown in Figure 1f and g, Pd nanowires with similar morphologies were also obtained from both ethylene glycol (EG) and triethylene glycol (TEG). It is well-known that the reducing power of a polyol is highly dependent on the length of its hydrocarbon chain. Specifically, the longer the hydrocarbon chain is, the weaker its reducing power will be. Thus, the reducing powers of the polyols should decrease in the order of EG>DEG>TEG.[15] Since products with essentially the same morphology were obtained from all these polyols, it can be concluded that the present protocol is robust enough for the synthesis of Pd ultrathin nanowires under a range of conditions. When the hydrocarbon chain of the polyol was further prolonged to, for example, tetraethylene glycol (TTEG), it was found that the obtained Pd nanowires were much shorter compared to the product obtained from DEG, together with the presence of some very small Pd particles (<2 nm) (Figure S2). This result indicated that small Pd nanoparticles could also be

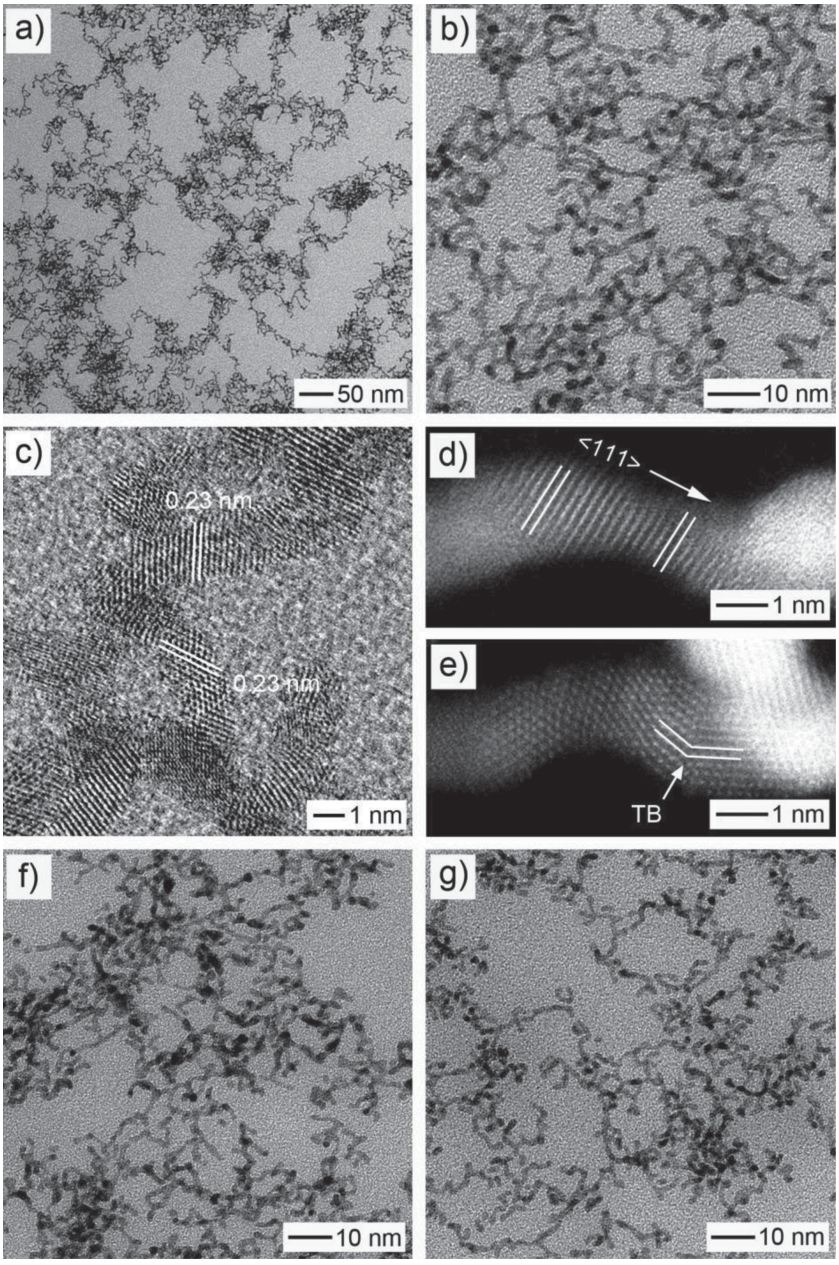

Figure 1. a,b) TEM images of a typical sample of Pd nanowires synthesized in DEG using the standard procedure; c) high-resolution BF-STEM image of the Pd nanowires; d,e) high-resolution HAADF-STEM images of the Pd nanowire; f,g) TEM images of Pd nanowires synthesized using the standard procedure except that the DEG was replaced by EG and TEG, respectively.

generated through the reduction by TTEG although it had relatively weaker reducing power. However, the relatively higher viscosity of TTEG might greatly reduce the diffusion rate of Pd nanoparticles and thus hinder their attachment and growth.[15b]

2.2. Nucleation and Attachment of Pd Nanoparticles

In order to understand how the Pd wavy nanowires were formed during a polyol synthesis, time-dependent evolution of the morphologies of the products were investigated by TEM imaging. As shown in **Figure 2**a, small Pd nanoparticles with diameters of 2–3 nm were formed at the initial stage (typically, within 1 min) of the synthesis, as marked by the white arrows. Some of the Pd nanoparticles also started to attach with each other to generate short nanowires less than 20 nm in length. In the next 9 min, essentially all the nanoparticles were attached to the pre-formed short nanowires, and no additional Pd nanoparticles were generated through homogeneous nucleation during this period of time (Figure 2b). This observation indicates that the kinetics of this reaction was very fast at the initial stage because the precursor could be completely depleted in 1 min due to the reduction by DEG. After 30 min, the short nanowires further attached end-to-end to generate elongated nanowires several tens to hundreds of nanometers (Figure 2c). It was found that the width of the longer nanowires was relatively smaller than that of the pre-formed, shorter ones or the diameter of the initial nanoparticles, suggesting that the Pd atoms could diffuse or migrate from the surfaces of the nanoparticles to the joint regions. Finally, the nanowires could interweave with each other to generate a two-dimensional (2D) network (Figure 2d). Combined together, our results clearly demonstrated that the formation of Pd wavy nanowires involved the following major steps: *i*) generation of small Pd nanoparticles 2–3 nm in diameter within 1 min through nucleation burst and complete depletion of the precursor; *ii*) collision and attachment of the small and thermodynamically unstable nanoparticles to generate relatively short nanowires; and *iii*) connection of the short nanowires via an end-to-end mode to generate longer nanowires and even 2D networks.

The time-dependent observations indicated that the formation of Pd nanowires involved a nucleation burst within a very short period of time and an attachment process over a relatively long period of time. Thus, controlling the reaction kinetics during the initial stage is significantly important to the formation of small and thermodynamically unstable nanoparticles and then the nanowires via attachment growth. As a parameter critical for the control of reduction kinetics, we systematically studied the effect of temperature on the formation of Pd nanowires. **Figure 3** shows TEM images of the products prepared using the standard procedure except for the difference in reaction temperature. It was observed that a great number of large particles (>10 nm) with irregular shapes were generated when the reaction temperature was set to 60 °C (Figure 3a). Although small

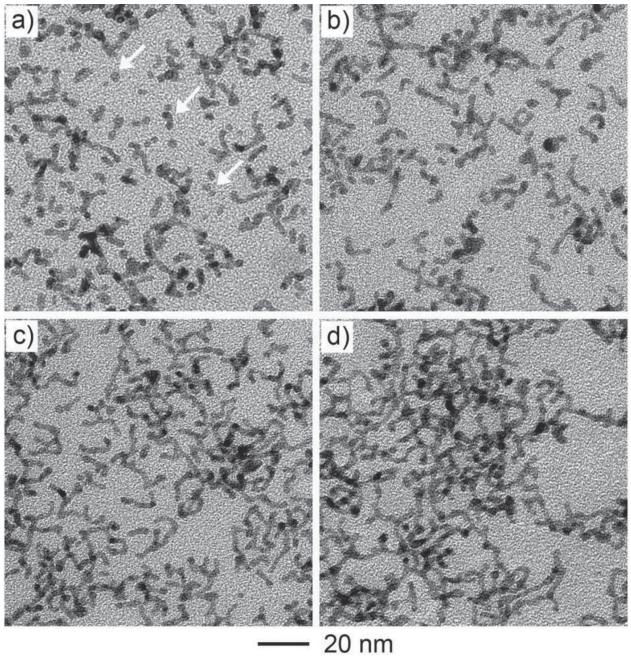

Figure 2. TEM images showing the attachment and time-dependent growth of Pd nanoparticles into wavy nanowires at 140 °C after the precursor had been injected: a) 1 min, b) 10 min, c) 30 min, and d) 3 h. The white arrows in (a) mark a few typical small Pd nanoparticles formed in the early stage of the synthesis.

nanoparticles and short nanowires could be obtained at 100 °C, there were also some larger particles coexisted in the system (Figure 3b). In contrast, large Pd particles disappeared and only nanowires were observed when the temperature was increased to 120 °C (Figure 3c). Longer and more uniform nanowires were obtained when the temperature was further increased to 140 and 160 °C (Figure 1b and 3d). These results demonstrated that the reaction temperature played an important role in the kinetic control of the nucleation and growth of Pd in the early stage of a synthesis. Specifically, a nucleation burst was able to take place in a very short period of time at a relatively high temperature (e.g., >120 °C in the present system). As a result, a large number of Pd nuclei could be generated, which then grew into small nanoparticles 2–3 nm in diameter. These particles with such small sizes were thermodynamically unstable due to the high surface energy. In order to minimize the total surface free energy, the facets with relatively high surface energies tend to contact with each other and coalesce during collision while the facets with lower energies remained to be exposed.[16] As such, Pd nanowires enclosed by facets with the lowest energy, {111} facets, were obtained. In contrast, we could only obtain much larger nanoparticles when the temperature was below 120 °C. These large particles could prevail in the system due to their relatively low surface energy compared with their smaller counterparts.

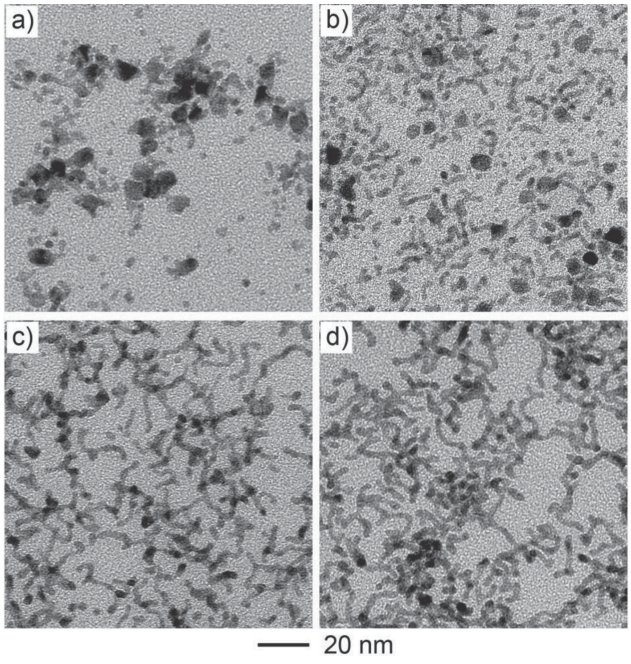

Figure 3. TEM images of Pd nanostructures prepared using the standard procedure, except for the change of reaction temperature from 140 °C to: a) 60, b) 100, c) 120, and d) 160 °C.

In addition to temperature and reductant/solvent, the effect of precursor on the reaction kinetics and thus the final morphology of the Pd nanostructures were also studied systematically. Previous reports have demonstrated that different Pd precursors involved distinct ligands to coordinate with Pd^{2+} and they could be reduced to Pd atoms at quite different rates.[17] As shown in **Figure 4**a–c, Pd nanostructures with different shapes and sizes were obtained under the same condition except for the use of different precursors. When we used $(CH_3COO)_2Pd$ as the precursor, Pd short nanowires could also be obtained via the attachment of small particles (Figure 4a). This result suggested that the similar structure of $(CF_3COO)_2Pd$ and $(CH_3COO)_2Pd$ allowed them to have similar reduction kinetics in a polyol system. However, the as-obtained nanowires from $(CH_3COO)_2Pd$ were much shorter and thicker than what were prepared from $(CF_3COO)_2Pd$, suggesting relatively slower reaction kinetics of $(CH_3COO)_2Pd$ than $(CF_3COO)_2Pd$. To confirm this argument, ascorbic acid (AA) was added as an additional reductant under the same condition to speed up the reaction. As expected, nanowires with elongated lengths and decreased diameters were obtained (Figure 4d).

When the precursor was switched to $PdCl_4^{2-}$, Pd polyhedrons rather than nanowires were obtained. Octahedrons with an average edge length of ~10 nm and twinned nanocrystals with a diameter of ~20 nm were obtained when we used Na_2PdCl_4 and H_2PdCl_4 as the precursors, respectively (Figure 4b and c). These results suggest that the reactions involving $PdCl_4^{2-}$ as the precursor had much slower reaction kinetics. **Figure 5** shows the conversions of $(CF_3COO)_2Pd$ and Na_2PdCl_4 into Pd atoms as a function of reaction time, respectively. The concentrations of the residual Pd^{2+} ions remaining in the reaction solution at different time points could be calculated by measuring their absorbance using UV-vis spectroscopy. It was found that the conversion of $(CF_3COO)_2Pd$ into Pd atoms via polyol reduction could be completed within a very short period of time. Specifically, more than 80% Pd^{2+} ions were converted into Pd atoms at t = 0.5 min, and this value could reach 97.5% at t = 1 min and

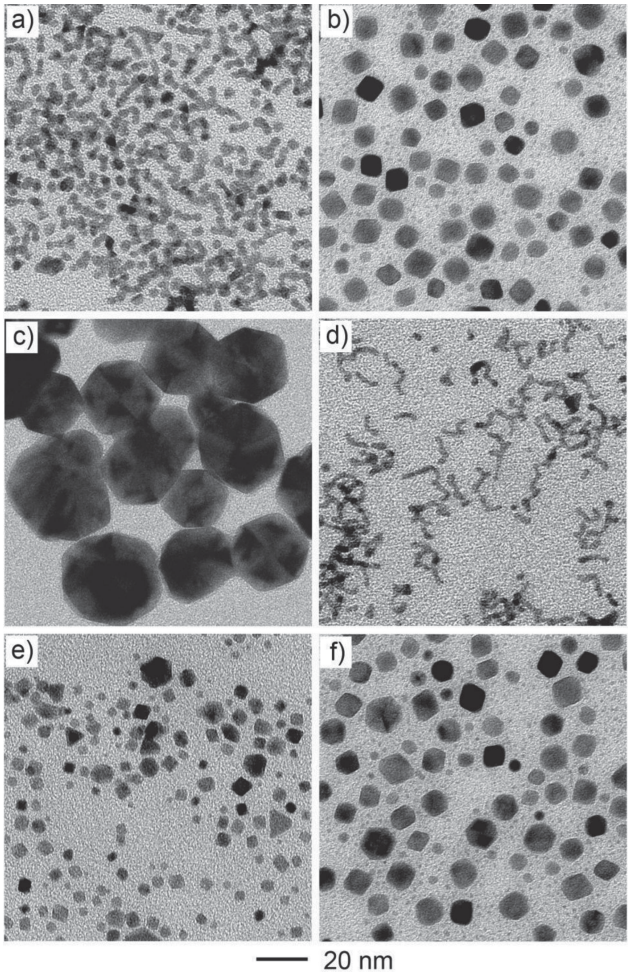

Figure 4. TEM images of Pd nanostructures prepared using the standard procedure, except for the use of different precursors or different combinations of starting materials: a) $(CH_3COO)_2Pd$, b) Na_2PdCl_4, c) H_2PdCl_4, d) $(CH_3COO)_2Pd$ + ascorbic acid, e) $(CF_3COO)_2Pd$ + NaCl, and f) Na_2PdCl_4 + CF_3COONa.

maintained a level approaching 100% thereafter. In contrast, the conversion of Na_2PdCl_4 into Pd atoms was much slower than the $(CF_3COO)_2Pd$ under the same condition. Only 6.9% Pd^{2+} ions were converted into Pd atoms at $t = 0.5$ min and then increased to 9.1%, 17.1%, 22.9%, 26.3%, 29.7%, 40.0%, and 50.3% at $t = 1$, 2, 3, 4, 5, 7.5, and 10 min, respectively. These observations indicated that different binding energies of the ligands (e.g., Cl^-, CF_3COO^-) with Pd^{2+} could significantly affect the reduction kinetics for converting Pd^{2+} into Pd atoms. This conclusion was also confirmed by the use of different combinations of precursors for the synthesis. As shown in Figure 4e, the ligand CF_3COO^- in the precursor of $(CF_3COO)_2Pd$ could be replaced by Cl^- and allowed to generate Pd polyhedrons. However, Cl^- in the precursor of Na_2PdCl_4 could not be replaced by CF_3COO^-, and thus the resultant products (as shown in Figure 4f) were essentially the same as what is shown in Figure 4b. In addition, oxidative etching might also play an important role in the formation of Pd polyhedrons when $PdCl_4^{2-}$ was used as the precursor. Our previous work has demonstrated that Pd

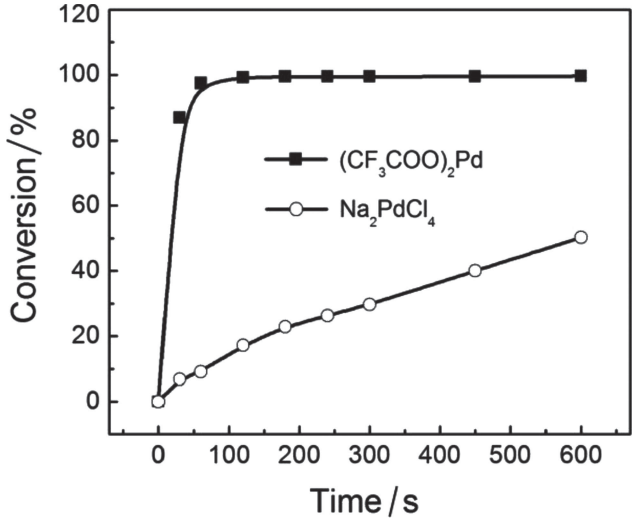

Figure 5. Plots showing the conversions of $(CF_3COO)_2Pd$ and Na_2PdCl_4 into Pd atoms as a function of reaction time, respectively.

particles involving twin defects could be removed more easily than single-crystal ones by oxidative etching due to their high surface energy.[18] Here, the twin defects generated at the joint regions via attachment of Pd nanoparticles could be destructed by oxidative etching when a large amount of Cl^- was involved in the synthesis. As a result, the attachment of Pd particles would be hindered and polyhedrons would be obtained. Combined together, we can conclude that the precursor used in the present work, $(CF_3COO)_2Pd$, played a critical role in the formation of Pd ultrathin nanowires.

2.3. Contribution of Surface Charge and Capping to Attachment

In addition to surface energy, surface charge and capping of Pd nanoparticles could also contribute to the attachment process. A large number of previous reports have already demonstrated the role(s) of these two parameters in stabilizing metal nanoparticles in hydrophilic systems.[19] We studied the surface properties of the as-obtained Pd nanowires using X-ray photoelectron spectroscopy (XPS) and zeta-potential measurement. As shown in **Figure 6**a and b, in addition to Pd 3d and 3p peaks, the signal of N 1s (400.1 eV) and C 1s (284.8 eV) were also observed in the survey spectra, indicating that PVP, a colloidal stabilizer, could still remain on the surfaces of the nanowires even after washing several times. Besides, no peak representing fluorine (the binding energy of F 1s is usually in the range of 684–689 eV, as shown in Figure 6b) was detected, suggesting that the ligand, CF_3COO^-, did not bind to the surfaces of the as-obtained nanowires after it had been released from the precursor. However, when the precursor was switched to $NaPdCl_4$, a new peak located at 198.0 eV was also observed (Figure 6c and d), which could be assigned to Cl 2p. This result suggested that both PVP and Cl^- could adsorb on the surfaces of the as-obtained Pd nanostructures when $NaPdCl_4$ was used as the precursor. In addition, the zeta-potential measurement revealed that the Pd nanostructures synthesized by using $(CF_3COO)_2Pd$

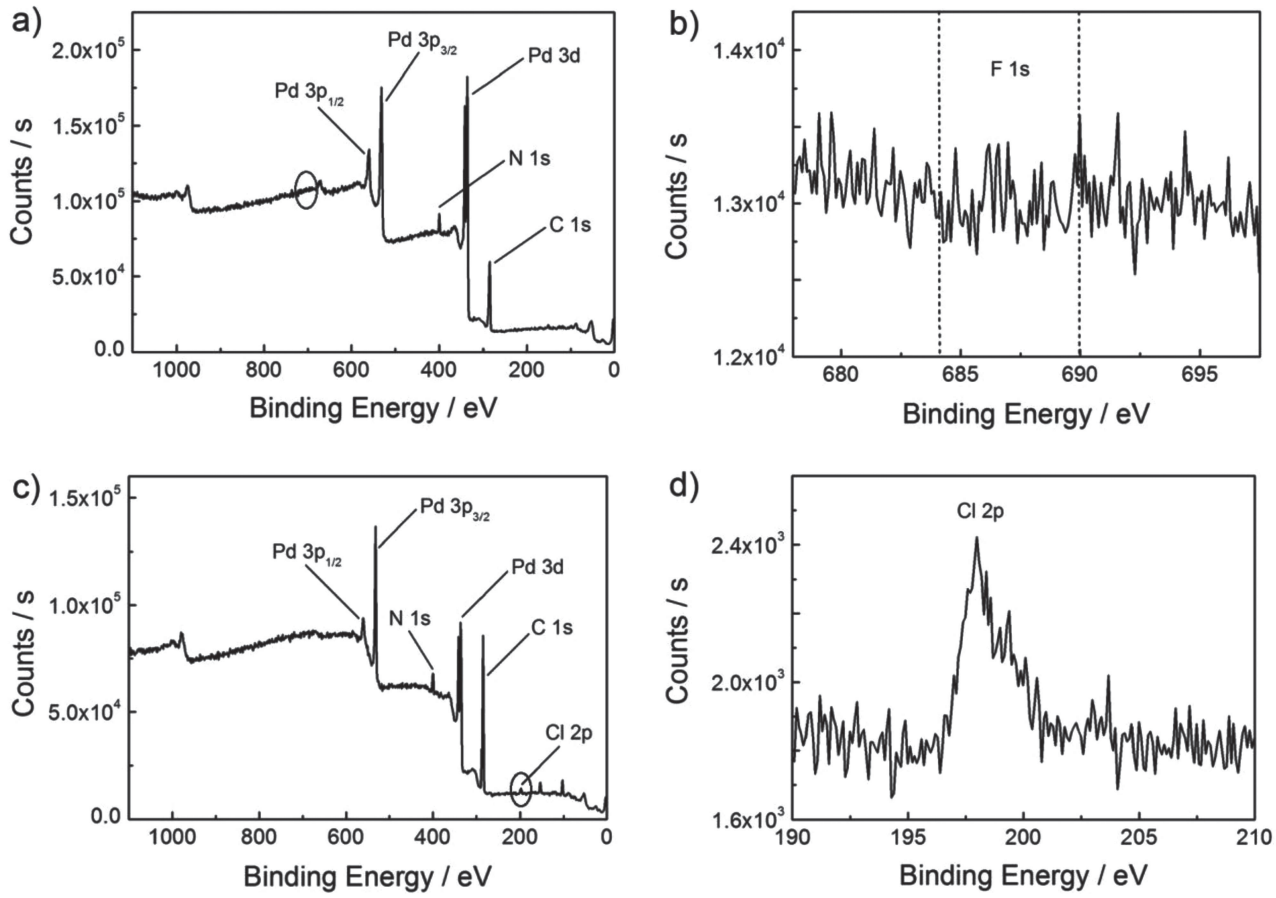

Figure 6. XPS spectra of Pd nanostructures prepared using the standard procedure, except for the use of different precursors for the synthesis: a,b) Pd nanowires prepared using $(CF_3COO)_2Pd$ as the precursor; and c,d) Pd polyhedrons prepared using Na_2PdCl_4 as the precursor.

and Na_2PdCl_4 as precursors had distinct surface charges. Specifically, the Pd nanowires prepared from $(CF_3COO)_2Pd$ showed a potential of –13.2 mV, while the Pd polyhedrons derived from $NaPdCl_4$ had a much lower potential of –28.7 mV. Obviously, such a difference in surface charge could be attributed to the absence or presence of negatively charged ligand (i.e., Cl^-) on their surfaces.

The results from XPS and zeta-potential measurements indicated that only PVP molecules were adsorbed on the surfaces of the Pd nanoparticles and nanowires when $(CF_3COO)_2Pd$ was used as the precursor. According to the Derjaguin-Landau-Verwey-Overbeek (DLVO) theory, the stabilization of a colloidal system can be based upon the following two mechanisms: *i*) the electrostatic repulsion by the surface-adsorbed ions derived from the starting materials or additives of the reaction, and *ii*) the steric repulsion due to the presence of bulky molecules (e.g., polymers or surfactants).[20] In the present work, the surface charge of the as-obtained Pd nanowires was essentially close to neutral due to the adsorption of PVP molecules only on their surfaces, suggesting that the inter-particle electrostatic repulsion would be too weak to overcome the Van der Waals attraction between the nanoparticles. On the other hand, it has been demonstrated that a proper amount of PVP can be introduced into polyol synthesis to prevent nanoparticles from aggregation. However, owing to its relatively large molecular weight and thus the steric hindrance effect, PVP could not effectively cap very small Pd nanoparticles of 2–3 nm in size. As a result, some facets of a Pd nanoparticle might not be protected against attachment. Short nanowires involving several nanoparticles could be obtained first, which could further grow in length via attachment with other particles or wires to generate relatively longer wires and even 2D networks. This mechanism was similar to a number of reports that used polymers or surfactants to achieve the anisotropic assembly of metal nanoparticles.[21] Combined together, it can be concluded that the following factors are important to the synthesis of ultrathin wavy nanowires: *i*) a nucleation burst in a very short period of time by fast reaction kinetics and thus generation of small nanoparticles with relatively high surface energy; and *ii*) low surface charge on the nanoparticles, which facilitates their attachment as driven by the Van der Waals force.

Figure 7 summarizes how the precursor-determined reaction kinetics affects the nucleation, growth, attachment, and thus the final morphology of the Pd nanostructures in a polyol synthesis. When $(CF_3COO)_2Pd$ was used as the precursor (top trace), a large number of Pd atoms could be generated within a very short period of time immediately after the precursor had been introduced, owing to the extremely fast reduction rate.

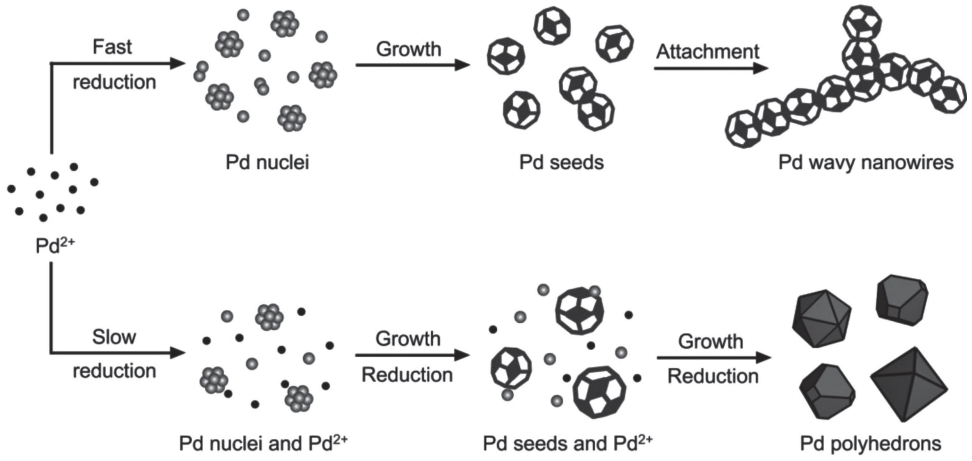

Figure 7. A schematic illustrating how the reaction kinetics (as mediated by precursor) affects the nucleation, growth, attachment, and thus the final morphology of Pd nanostructures in the polyol synthesis.

Once the concentration of Pd atoms had reached the level of supersaturation, they started to aggregate into nuclei (i.e., small clusters) through homogeneous nucleation. Then, the resultant Pd nuclei could only grow into relatively small Pd particles of 2–3 nm in size because the nucleation burst had consumed essentially all the precursors. Owing to the relatively high surface energy and low surface charge, the as-formed Pd nanoparticles tended to attach to each other in order to minimize the total surface free energy of the system, resulting in the formation of Pd wavy nanowires. In contrast, when the precursor was switched to Na_2PdCl_4 (bottom trace), the relatively slow reduction rate of this halogen-coordinated precursor allowed the nucleation and growth of Pd nanoparticles to take place over a much longer period of time.[17] In this case, fewer Pd nuclei and thus Pd nanoparticles were formed in comparison with the case that used $(CF_3COO)_2Pd$ as the precursor. As such, the Pd atoms generated through slow reduction of the Na_2PdCl_4 could be continuously deposited onto the existing Pd seeds through heterogeneous nucleation, allowing them to grow into larger particles with relatively lower surface energy. In addition, the Cl^- derived from the precursor could adsorb onto the surfaces of the resultant Pd nanoparticles, leading to a higher surface charge and thus stronger electrostatic repulsion between the nanoparticles. As a result, well-dispersed Pd polyhedrons with much larger sizes were obtained.

2.4. Catalytic Activity of the Pd Ultrathin Nanowires

The as-prepared Pd nanowires were further loaded on a carbon support to generate a new catalyst (i.e., Pd NWs/C containing 10 wt% Pd). It was found that the nanowires loaded on carbon were relatively shorter in length than the original ones (Figure S3a), which might be attributed to the long-time sonication during the loading process. The electrocatalytic activity of the Pd NWs/C catalyst was then studied using the FOR reaction as a model system, together with the conventional Pd/C (10 wt% Pd) being tested under the same condition for comparison. Electrochemical cyclic voltammograms (CVs) were used to characterize the activity of these Pd catalysts. The curves of Cu underpotential deposition (Cu_{UPD}, see Figure S4) were measured in a N_2-saturated aqueous solution containing 0.05 M H_2SO_4 and 0.05 M $CuSO_4$ at a scan rate of 5 mV s^{-1}. The electrochemically active surface areas (ESAs) of the catalysts could be calculated by integrating the stripping charges of a Cu_{UPD}, which corresponded to 460 μC cm^{-2} for both Pd NWs/C and Pd/C with polycrystalline Pd surfaces.[22] The ESA values of Pd NWs/C and Pd/C were 59.3 and 60.2 m^2 g_{Pd}^{-1}, respectively, confirming the similarities in size and thus surface area for the as-prepared Pd NWs/C and the conventional Pd/C catalyst.

Figure 8 shows the CVs of these two types of catalysts for FOR. The current densities (j / mA cm^{-2}) were normalized to the ESAs of the catalysts derived from the Cu_{UPD} charges. The forward sweep (Figure 8a) showed that the anodic potential peaks of Pd NWs/C and conventional Pd/C catalysts were positioned at 0.64 and 0.60 V, with current densities of 2.4 and 0.7 mA cm^{-2}, respectively. It is known that the electrocatalysis of FOR has two different decomposition pathways. One is the direct dehydrogenation pathway dominating at relatively low overpotentials, and the other is an indirect dehydration pathway, which can lead to the catalytic poisoning at relatively high overpotentials due to CO adsorption on Pd.[22] Here, the current density of Pd NWs/C was 2.5 times higher than that of Pd/C (1.08 vs. 0.44 mA cm^{-2}) at 0.4 V (a practical potential of direct formic acid fuel cell, vs. RHE), demonstrating that the present Pd NWs/C catalyst had better performances over the conventional Pd/C for FOR. In addition, it was found that the current density of Pd NWs/C sharply increased at about 0.8 V during the backward sweep (Figure 8b), indicating that the catalytic activity of the Pd NWs/C could be quickly recovered, probably through hydrogenation of the oxidized species adsorbed on their surfaces.[23]

It is widely recognized that the catalytic activity for FOR reaction is highly dependent on the particle size.[24] Here, the effect of particle size could be neglected because these two types of catalysts had similar sizes (2 nm in width for the nanowires and 2–3 nm in diameter for the Pd particles involved in Pd/C).

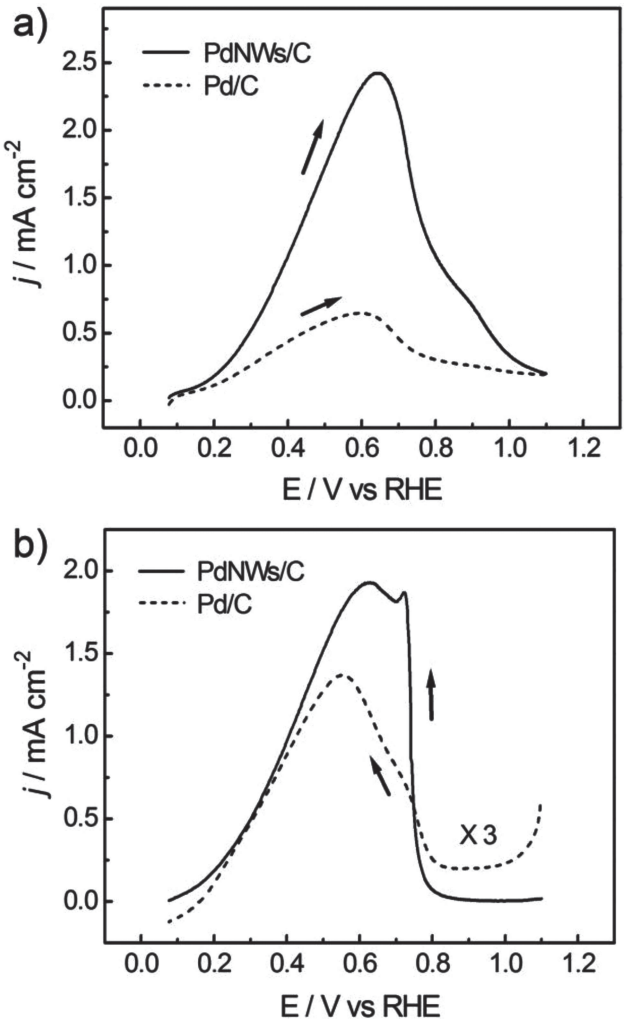

Figure 8. Cyclic voltammograms of formic acid oxidation over two different Pd catalysts: a) the forward sweep and b) the backward sweep. The Pd NWs/C catalyst was prepared by loading the Pd wavy nanowires on a carbon support (10 wt% of Pd), and a conventional Pd/C with the same Pd content was also measured for comparison. The data were collected at room temperature in an aqueous solution containing HCOOH (2 M) and $HClO_4$ (0.1 M) at a scan rate of 50 mV s^{-1}. RHE = reversible hydrogen electrode.

Our recent study demonstrated that the twin defects involved in the Pd nanocrystals could play an important role in the improvement of electrocatalytic activity towards FOR.[25] Thus, the higher catalytic activity of Pd NWs/C relative to conventional Pd/C towards the FOR can be attributed to their unique wavy, wire-like structure and the inclusion of numerous twin defects. In addition, it was found that the wire-like shape was essentially retained after the Pd NWs/C had been used for catalyzing the FOR (Figure S3b), suggesting good stability of the as-prepared Pd nanowires.

3. Conclusion

We have successfully demonstrated the synthesis of Pd ultrathin nanowires in high purity by manipulating the reaction kinetics to promote the attachment-based growth. Our mechanistic studies indicate that the success of this synthesis relies on two major parameters: a fast reaction kinetics during the nucleation stage and low surface charge of the small Pd particles generated at the early stage, both enabled by the precursor, $(CF_3COO)_2Pd$, used for the synthesis. Specifically, the precursor could be reduced instantaneously to generate a very large number of small Pd particles of 2–3 nm in diameter. Due to a quick depletion of precursor, the small particles were unable to grow in size through atomic addition. Instead, they were forced to coalesce into ultrathin nanowires with a wavy morphology via an attachment mechanism in the case of a low surface charge. Thanks to the unique wavy, wire-like structure and involvement of twin defects, the as-prepared Pd ultrathin nanowires showed a catalytic current density of 2.5 times higher than the conventional Pd/C catalyst towards FOR. We believe this work will offer plenty of inspiration and strategies for the rational design and fabrication of novel metal nanostructures through attachment-based growth for a broad range of applications.

4. Experimental Section

Chemicals and Materials: $(CF_3COO)_2Pd$ (97%), $(CH_3COO)_2Pd$ (≥99.9%), Na_2PdCl_4 (98%), $PdCl_2$ (≥99.9%), Pd nanoparticles supported on carbon (the conventional Pd/C catalyst, 10 wt%), CF_3COONa (98%), diethylene glycol (DEG, 99%), triethylene glycol (TEG, 99%), tetraethylene glycol (TTEG, 99%), poly(vinyl pyrrolidone) (PVP, $M_W \approx$ 55,000), NaCl, L-ascorbic acid (AA), and acetone were all obtained from Sigma-Aldrich. Ethylene glycol (EG, lot no. K43B24) was obtained from J. T. Baker. All chemicals were used as received. Deionized (DI) water with a resistivity of 18.2 MΩ·cm was used for all the experiments.

Synthesis of Pd Ultrathin Nanowires: In a standard synthesis, PVP (30 mg) and DEG (2 mL) were added into a glass vial and heated in an oil bath at 140 °C under magnetic stirring. Then, another DEG solution (1 mL) containing $(CF_3COO)_2Pd$ (10 mg) was quickly injected with a pipette. The vial was removed from the oil bath 3 h later and naturally cooled down to room temperature. After centrifugation and washing with acetone and DI water, the product was re-dispersed in DI water (3 mL). Other types of Pd nanostructures were also prepared using the standard procedure except for the use of different precursors or different combinations of starting materials, which are described in detail in the Results and Discussion section.

Electrochemical Measurements: Pd NWs/C (10 wt% of Pd nanowires loaded on carbon, 2 mg) and the conventional Pd/C catalyst (10 wt% of Pd particles on carbon, 2 mg) were dispersed in DI water (1 mL) and treated by ultrasonic for 10 min, respectively. Then, Nafion aqueous solution (5%, 30 μL) was added and the mixtures were subjected to ultrasonic treatment for 10 min again. To prepare the working electrode, an aqueous suspension of the catalyst (10 μL) was dropped onto the pre-cleaned glassy carbon electrode (Bioanalytical Systems Inc., United States) and then allowed to dry in an oven at 70 °C for 10 min. To remove PVP on the surface of the catalyst, the electrode potential was held at -0.05 V (vs. RHE) for 60 s.[22] An Ag/AgCl electrode and a Pt mesh were used as the reference and counter electrodes, respectively. The potentials are reported relative to RHE. To obtain FOR activity, two cycles for each measurement were conducted in a N_2-saturated aqueous solution containing $HClO_4$ (0.1 M) and HCOOH (2 M) at a scan rate of 50 mV s^{-1}. The Cu_{UPD} was conducted in an aqueous solution containing H_2SO_4 (50 mM) and $CuSO_4$ (50 mM).

Characterizations: TEM images were taken using a JEM-1400 microscope (JEOL, Japan) operated at 120 kV by drop casting the nanoparticle dispersions on carbon-coated Cu grids and drying under

ambient conditions. High-resolution HAADF-STEM and BF-STEM images were obtained using an aberration corrected FEI-Titan 80/300S S/TEM microscope operated at 300 kV. XPS spectra were taken using a K-Alpha X-ray Photoelectron Spectrometer (Thermo Scientific, USA). Zeta-potential of the Pd nanostructures were measured using a Zetasizer Nano-ZS System (Malvern Inc.). XRD pattern of the Pd nanowires was obtained using a diffractometer (Paralytical XRD-600) operated at 40 kV and 40 mA with filtered Cu Kα radiation of 0.154 nm. UV-vis absorption spectra were recorded using a Lambda 750 UV-vis-NIR spectrometer (Perkin-Elmer, Waltham, MA). The concentrations of the Pd catalysts were determined using a Perkin Elmer inductively coupled plasma mass spectrometry (ICP-MS, NexION 300Q).

Supporting Information

Supporting Information is available from the Wiley Online Library or from the author.

Acknowledgements

This work was supported in part by a grant from NSF (DMR-1215034) and startup funds from Georgia Institute of Technology. As jointly supervised Ph.D. candidates, Y.W. (from Southwest University) and S.X. (from Xiamen University) were also partially supported by Fellowships from the China Scholarship Council (CSC). Part of the electron microscopy work was performed at ORNL's Shared Research Equipment (ShaRE) User Program sponsored by DOE-BES.

Received: July 11, 2013
Published online: August 19, 2013

[1] a) R. Jin, Y. Cao, C. A. Mirkin, K. L. Kelly, G. C. Schatz, J. G. Zheng, *Science* **2001**, *294*, 1901; b) Y. Sun, Y. Xia, *Science* **2002**, *298*, 2176; c) C. J. Murphy, N. R. Jana, *Adv. Mater.* **2002**, *14*, 80; d) C. Burda, X. Chen, R. Narayanan, M. A. El-Sayed, *Chem. Rev.* **2005**, *105*, 1025; e) C. Wang, H. Daimon, T. Onodera, T. Koda, S. Sun, *Angew. Chem. Int. Ed.* **2008**, *47*, 3588; f) X. Liu, D. Wang, Y. Li, *Nano Today* **2012**, *7*, 448.

[2] a) V. K. LaMer, R. H. Dinegar, *J. Am. Chem. Soc.* **1950**, *72*, 4847; b) A. R. Tao, S. Habas, P. Yang, *Small* **2008**, *4*, 310; c) Y. Xia, Y. Xiong, B. Lim, S. E. Skrabalak, *Angew. Chem. Int. Ed.* **2009**, *48*, 60.

[3] a) W. Ostwald, *Phys. Chem.* **1897**, *22*, 289; b) P. Dagtepe, V. Chikan, *J. Phys. Chem. C* **2010**, *114*, 16263; c) S. T. Gentry, S. F. Kendra, M. W. Bezpalko, *J. Phys. Chem. C* **2011**, *115*, 12736.

[4] R. L. Penn, J. F. Banfield, *Science* **1998**, *281*, 969.

[5] a) Z. Tang, N. A. Kotov, M. Giersig, *Science* **2002**, *297*, 237; b) Y. Jun, M. F. Casula, J.-H. Sim, S. Y. Kim, J. Cheon, A. P. Alivisatos, *J. Am. Chem. Soc.* **2003**, *125*, 15981; c) K.-S. Cho, D. V. Talapin, W. Gaschler, C. B. Murray, *J. Am. Chem. Soc.* **2005**, *127*, 7140; d) J. H. Yu, J. Joo, H. M. Park, S.-I. Baik, Y. W. Kim, S. C. Kim, T. Hyeon, *J. Am. Chem. Soc.* **2005**, *127*, 5662; e) D. Li, M. H. Nielsen, J. R. I. Lee, C. Frandsen, J. F. Banfield, J. J. De Yoreo, *Science* **2012**, *336*, 1014; f) W. H. Evers, B. Goris, S. Bals, M. Casavola, J. de Graaf, R. van Roij, M. Dijkstra, D. Vanmaekelbergh, *Nano Lett.* **2013**, *13*, 2317.

[6] a) L. Lu, A. Kobayashi, Y. Kikkawa, K. Tawa, Y. Ozaki, *J. Phys. Chem. B* **2006**, *110*, 23234; b) X. Wen, Y.-T. Xie, M. W. C. Mak, K. Y. Cheung, X.-Y. Li, R. Renneberg, S. Yang, *Langmuir* **2006**, *22*, 4836.

[7] H. Liang, H. Zhao, D. Rossouw, W. Wang, H. Xu, G. A. Botton, D. Ma, *Chem. Mater.* **2012**, *24*, 2339.

[8] A. Halder, N. Ravishankar, *Adv. Mater.* **2007**, *19*, 1854.

[9] C. Zhu, H.-C. Peng, J. Zeng, J. Liu, Z. Gu, Y. Xia, *J. Am. Chem. Soc.* **2012**, *134*, 20234.

[10] Z. Peng, H. You, H. Yang, *ACS Nano* **2010**, *4*, 1501.

[11] X. Yu, D. Wang, Q. Peng, Y. Li, *Chem. Eur. J.* **2013**, *19*, 233.

[12] B. Y. Xia, H. B. Wu, Y. Yan, X. W. Lou, X. Wang, *J. Am. Chem. Soc.* **2013**, *135*, 9480.

[13] H.-G. Liao, L. Cui, S. Whitelam, H. Zheng, *Science* **2012**, *336*, 1011.

[14] H. Zhang, X. Xia, W. Li, J. Zeng, Y. Dai, D. Yang, Y. Xia, *Angew. Chem. Int. Ed.* **2010**, *49*, 5296.

[15] a) C.-L. Lee, C.-C. Wan, Y.-Y. Wang, *Adv. Funct. Mater.* **2001**, *11*, 344; b) Y. Wang, Y. Zheng, C. Z. Huang, Y. Xia, *J. Am. Chem. Soc.* **2013**, *135*, 1941.

[16] Q. Zhang, S.-J. Liu, S.-H. Yu, *J. Mater. Chem.* **2009**, *19*, 191.

[17] a) X. Huang, H. Zhang, C. Guo, Z. Zhou, N. Zheng, *Angew. Chem. Int. Ed.* **2009**, *48*, 4808; b) Y. Wang, S. Xie, J. Liu, J. Park, C. Z. Huang, Y. Xia, *Nano Lett.* **2013**, *13*, 2276.

[18] Y. Xiong, J. Chen, B. Wiley, Y. Xia, *J. Am. Chem. Soc.* **2005**, *127*, 7332.

[19] L. D. Pachón, G. Rothenberg, *Appl. Organometal. Chem.* **2008**, *22*, 288.

[20] A. Roucoux, J. Schulz, H. Patin, *Chem. Rev.* **2002**, *102*, 3757.

[21] a) Y. Yang, S. Matsubara, M. Nogami, J. Shi, W. Huang, *Nanotechnology* **2006**, *17*, 2821; b) L. Wu, C. Shi, L. Tian, J. Zhu, *J. Phys. Chem. C* **2008**, *112*, 319; c) Y. Wang, Y. F. Li, C. Z. Huang, *J. Phys. Chem. C* **2009**, *113*, 4315; d) Y. Wang, L. Q. Chen, Y. F. Li, X. J. Zhao, L. Peng, C. Z. Huang, *Nanotechnology* **2010**, *21*, 305601.

[22] M. Shao, J. Odell, M. Humbert, T. Yu, Y. Xia, *J. Phys. Chem. C* **2013**, *117*, 4172.

[23] a) H. Miyake, T. Okada, G. Samjeské, M. Osawa, *Phys. Chem. Chem. Phys.* **2008**, *10*, 3662; b) Y. Suo, I.-M. Hsing, *Electrochim. Acta* **2009**, *55*, 210.

[24] a) W. P. Zhou, A. Lewera, R. Larsen, R. I. Masel, P. S. Bagus, A. Wieckowski, *J. Phys. Chem. B* **2006**, *110*, 13393; b) W. Zhou, J. Y. Lee, *J. Phys. Chem. C* **2008**, *112*, 3789.

[25] T. Lv, Y. Wang, S.-I. Choi, M. Chi, J. Tao, L. Pan, C. Z. Huang, Y. Zhu, Y. Xia, *ChemSusChem* **2013**, DOI: 10.1002/cssc.201300479.